

The Multiscale Bowler-Hat Transform for Vessel Enhancement in 3D Biomedical Images

BMVC 2018 Submission # 314

Abstract

Enhancement and detection of 3D vessel-like structures has long been an open problem as most existing image processing methods fail in many aspects, including a lack of uniform enhancement between vessels of different radii and a lack of enhancement at the junctions. Here, we propose a method based on mathematical morphology to enhance 3D vessel-like structures in biomedical images. The proposed method, 3D bowler-hat transform, combines sphere and line structuring elements to enhance vessel-like structures. The proposed method is validated on synthetic and real data, and compared with state-of-the-art methods. Our results show that the proposed method achieves a high-quality vessel-like structures enhancement in both synthetic and real biomedical images, and is able to cope with variations in vessels thickness throughout vascular networks while remaining robust at junctions.

1 Introduction

Automatic detection of vessel-like structures is one of the fundamental procedures in many 3D biomedical image processing applications, where they are used to understand important vascular networks, such as cytoskeletal networks, blood vessels, airways, and other similar fibrous tissues. Reliable detection and then accurate analysis of these vascular networks strongly relies on robust vessel-like structures enhancement methods. Several such methods have been proposed and investigated for various types of biomedical images such as: blood vessels [1, 2], neurons [3], microtubules [4] and others [5, 6]. Nevertheless, most of the vessel-like structures enhancement methods still suffer from unresolved problems such as losing signals at the junctions or false vessel effects [7].

In this paper, we extended 2d vessel-like structures enhancement method to 3D, is called the 3D bowler-hat transform. The proposed method is based on a recently developed 2D image filtering method exploring a concept of mathematical morphology [8]. We qualitatively and quantitatively validate and compare the proposed method with the state-of-the-art methods using a range of synthetic and real biomedical images. Our results show that the proposed method produces a high-quality vessel enhancement, especially at junctions in both synthetic and real images. The method is suitable to be applied to a variety of biomedical image types without requiring prior preparation or tuning. Finally, we make our method available online, along with source code and all test functions.

2 Related Work

A considerable amount of work has been conducted on the enhancement and segmentation of vessel-like structures [13, 51]. In this section we summarise them into three categories: Hessian-based enhancement, phase-congruency-based enhancement, and morphological enhancement, and the representative state-of-the-art works are reviewed under each categories.

2.1 Hessian-based Enhancement Methods

Frangi et al. [14] proposed 2/3D vessel-like structures enhancement in biomedical images by exploring the relationships between eigenvectors and eigenvalues of a Hessian matrix. The Hessian is constructed with responses of a set of matching filters, defined by second-order derivatives of the Gaussian function, convolved with the image. Three most common measurements proposed to date are vesselness, neuriteness and regularized volume ratio.

2.1.1 Vesselness

Vesselness measure [14] is a function of the eigenvalues of the Hessian matrix of the image data. The eigenvalues of the Hessian matrix correspond to the second derivatives of the image data in the direction of the associated eigenvector. In general, vesselness fails at vessels junctions due to the low filters responses.

2.1.2 Neuriteness

As an alternative to vesselness, neuriteness measure modifies the Hessian matrix by adding a new parameter to improve vessel-like structures enhancement in 2D biomedical images [15]. This work was then extended for use in 3D biomedical images by [16]. Neuriteness, in the same way as the vesselness, fails at vessels junctions due to the low filters responses.

2.1.3 Regularized Volume Ratio

A problem with Hessian-based methods such as vesselness or neuriteness is the direct proportionality of the output to the eigenvalues. Due to eigenvalue heterogeneity within objects and variation in eigenvalue magnitude, this proportionality results in non-uniform enhancement. In [17], authors attempt to solve this problem by deriving a modification of the volume ratio with a regularised eigenvalue to ensure robustness to small changes in magnitude.

2.2 Phase Congruency-based Enhancement Methods

Most image enhancement methods have a common problem of image contrast and spatial magnification dependency, which causes low contrast vessels to be missed [18, 16]. To overcome this problem, [20] proposes a contrast-independent image features enhancement method exploring a concept called a phase congruency. The phase congruency compares the weighted alignment of the Fourier components of the image with the sum of the Fourier components [8, 19].

In similar way as with the Hessian matrix concept, a Phase Congruency Tensor (PCT) is proposed to represent local structures in the image; first in 2D by [22] and then in 3D by [24]. Then, eigenvalues and eigenvectors of the PCT are calculated and used to define PCT vesselness and PCT neuriteness. A major drawback of phase-based methods is the complexity of the parameter space to calculate the PCT.

2.3 Enhancement with Mathematical Morphology

Another class of image enhancement methods is based on mathematical morphology, which has been used for several challenges [9, 11, 21, 23]. To enhance vessel-like structures, Zana and Klein [30] propose the use of morphological transforms. This method assumes

092 that vessels are linear, connected and have smooth variations of curvature along the peak
 093 of the structure. First, a sum of top-hats is computed using linear structuring elements at
 094 different angles; then a curvature measure is calculated using a Laplacian of Gaussian, and
 095 finally, both of them are combined to reduce noise and enhance vessel-like structures in an
 096 image. Recently, another mathematical morphology-based method proposed that is called
 097 Ranking the Operation Responses of Path Operators (RORPO) [19]. It is designed to filter
 098 out planar and blob-like structures by identifying curvilinear structures in 3D images. The
 099 main disadvantage of this method is its high computation cost when applied to large volume
 100 image datasets.

101 2.4 Limitations and Challenges

103 Many vessel-like structure enhancement methods still fail in ways that compromise their
 104 use in automated detection and analysis pipelines. For example, contrast variations cause
 105 low-accuracy enhancement, and high noise levels lead to the poor enhancement and the
 106 'false vessel' effect. Another common issue is dealing with junctions, where most Hessian-
 107 or PCT-based methods suppress the 'disk-like' features at a junction leading to a loss of
 108 extracted network connectivity. Further, some methods are computationally expensive or
 109 have a complex set of parameters that can be time-consuming to manually fine-tune.

110 3 Method

112 In this section, we introduce a 3D extension of a recently introduced mathematical morphology-
 113 based 2D method for vessel-like structure enhancement called the bowler-hat transform [25].
 114 While explaining the details of the proposed method, we point out the concepts that allow us
 115 to address the major drawbacks of existing, state-of-the-art vessel-like structures enhance-
 116 ment methods.

117 3.1 Mathematical Morphology

119 Mathematical morphology has been extensively used in image processing and image anal-
 120 ysis [26, 27]. Mathematical morphology uses structuring elements and concepts from set
 121 theory to describe features of interest in images. Most morphological operations are based
 122 on two basic operations: dilation and erosion. These two operations take the image as an
 123 input and dilate or erode components within the particular area with structuring element.
 124 While erosion extends dark areas decreasing bright areas, dilation expands bright areas and
 125 decrease dark areas.

126 Using these two operators, two further operations can be defined, that are called opening and
 127 closing. The closing preserves bright structures while suppressing dark patterns meantime
 128 the opening maintains dark structures and patterns and suppressing bright features.

129 3.2 Proposed Method

131 The 3D bowler-hat transform combines two banks of different structuring elements: a bank
 132 of spherical structuring elements with varying diameter and a bank of orientated line struc-
 133 turing elements with varying length and directions.

134 First, we create a bank of morphological openings of a 3D input image I with spherical
 135 structuring elements S_{sphere}^d of diameter $d \in [1, d_{max}]$, where d_{max} is expected maximum size
 136 of vessel-like structures in a given image I . After every morphological opening of the image
 137 I , vessel-like structures smaller than d are eliminated and the ones larger than d remain.

As a result, a 3D image stack, for all $d \in [1, d_{max}]$, is constructed as:

$$\{I_{sphere}\} = \{I \circ S_{sphere}^d\}, \quad \forall d \in [1, d_{max}]. \quad (1)$$

Then, another bank of morphological openings of the input image I is performed with line structuring elements $S_{line}^{d,v}$ of lengths d , $\forall d \in [1, d_{max}]$, and of directions defined as follows:

$$\mathbf{v} = (\theta_k, \phi_k), \quad \forall k \in [1, N]. \quad (2)$$

Direction (θ_k, ϕ_k) is defined as a k^{th} point from N uniformly distributed points on the unit sphere, and more details can be found in [14]. After every morphological opening of the image I with a line structuring element $S_{line}^{d,v}$, vessel-like structures smaller than d along direction \mathbf{v} are eliminated but all vessel-like structures that are longer than d along direction \mathbf{v} remain. This step results in a 3D image stack for all lengths d and all directions \mathbf{v} :

$$\{I_{line}\} = \{I \circ S_{line}^{d,v}\}, \quad \forall d \in [1, d_{max}], \forall k \in [1, N]. \quad (3)$$

Then, for each length d , a pixel-wise maximum across all directions \mathbf{v} is calculated resulting in a 3D image stack:

$$\{I_{line}\} = \left\{ \max_{k \in [1, N]} | \{I \circ S_{line}^{d,v}\} | \right\}, \quad \forall r \in [1, d_{max}]. \quad (4)$$

The enhanced image is then produced by taking maximum stack-wise difference at each pixel,

$$I_{enhanced} = \max_{r \in [1, d_{max}]} | \{I_{sphere} - I_{line}\} |. \quad (5)$$

With the 3D bowler-hat transform, areas that are dark (background) in the original image remain dark due to the use of openings; blob-like bright objects (undesired foreground features) are suppressed as the sphere-based and line-based opening gives similar values; and tube-like bright objects (desired foreground features) are enhanced due to the large difference between sphere-based and longer line-based openings. To assign an appropriate d_{max} , expected maximum vessel-like structures size in the image, allows the identification of most of the vessel-like structures and junctions, something that many other vessel enhancement methods fail to do. This is due to the ability to fit longer line-based structural elements within the junction area. In Section 4 we illustrate the key advantages of the proposed method over other vessel-like structure enhancement methods.

4 Results and Discussions

In this section, we qualitatively and quantitatively validate the efficiency of the proposed method using a range of synthetic and real biomedical image datasets. We then compare the proposed method with the state-of-the-art vessel-like structure enhancement methods such as Hessian-based vesselness [15], neuriteness [16] and volume ratio [17], PCT-based vesselness and neuriteness [18], and recently published RORPO [19].

4.1 Quantitative Validation

While a visual examination can give some subjective information regarding the effectiveness of the vessel enhancement method, a form a quantitative validation is also required. To compare the proposed method with the other state-of-the-art algorithms, we have chosen to calculate the Receiver Operating Characteristic (ROC) curve and the Area Under the Curve (AUC) and more details can be found in [20].

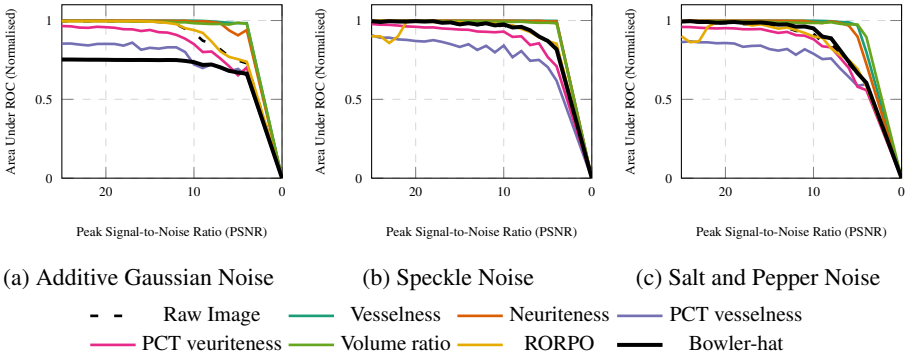


Figure 1: AUC values for the input image and the image enhanced by the proposed method and the state-of-the-art methods with different peak signal-to-noise ratios (PSNRs) for three different noise types: (a) additive Gaussian noise, (b) multiplicative Gaussian (speckle) noise, and (c) salt and pepper noise (see legend for colours).

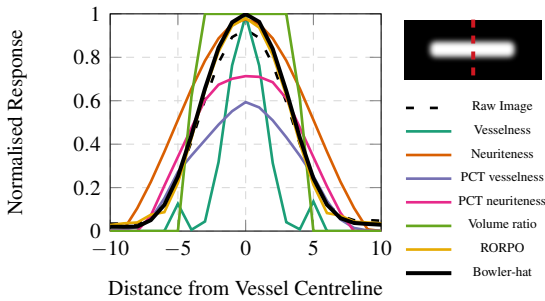


Figure 2: Cross-sectional profile of 2D max intensity projection of 3D synthetic vessel image (black, dashed line), vessel-like structure enhanced by the proposed method (black, solid line) and by the state-of-the-art methods (see legend for colours). All images were normalised such that the brightest pixel in the whole image has a value of 1 and the darkest a value of 0.

4.2 Response to Noise

Figure 1 presents the performance comparison of the proposed method with the state-of-the-art approaches under the influence of three different noises: additive Gaussian, speckle and salt & pepper. Evidently, the proposed method has no built-in noise suppression; as expected that the effect of noise on the enhanced image is in-line with the raw image. This inherits from the noise-sensitivity in mathematical morphological and should be taken into consideration while choosing an enhancement method.

4.3 Profile Analysis

Figure 2 illustrates bowler-hat and state-of-the-art methods responses to a simple vessel-like structure on a synthetic image. It is obvious that the value of the enhanced image at the middle of the vessel reaches a peak value and quickly drops off and decreases at the expected thickness of the vessel by the Hessian-based methods. On the other hand, the PCT-based methods are less responsive to the centreline of the vessel, while obtaining a high response to the edges due to the contrast variations. The value of the enhanced image does not significantly peak at the vessel centre, but their response does not drop off quickly since it is free from the contrast variations. The proposed method has both these benefits: a maximal peak value at the vessel centre-line and an enhanced response to the edges of the vessel. As a result, the reliable vessel thicknesses can be captured.

4.4 Response to Uneven Background Illumination

Figure 3 presents an intuitive comparison between the proposed method and other state-of-the-art methods, regarding the response to the uneven background illumination. When compared with the other methods, the proposed method maintains the high responses at the junctions and seems unaffected by uneven background illuminations.

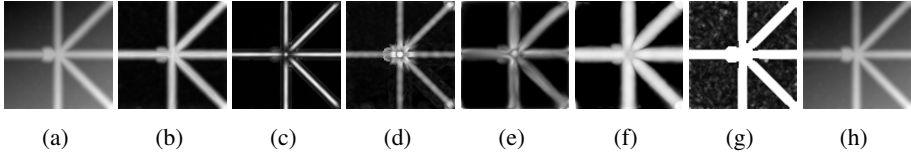
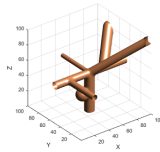


Figure 3: Comparison of the methods' abilities to deal with uneven background illumination. (a) The original image, (b) the bowler-hat, and state-of-the-art methods respectively; (c) vesselness, (d) neuriteness, (e) PCT vesselness, (f) PCT neuriteness, (g) volume ratio, and (h) RORPO.



(a) Input image

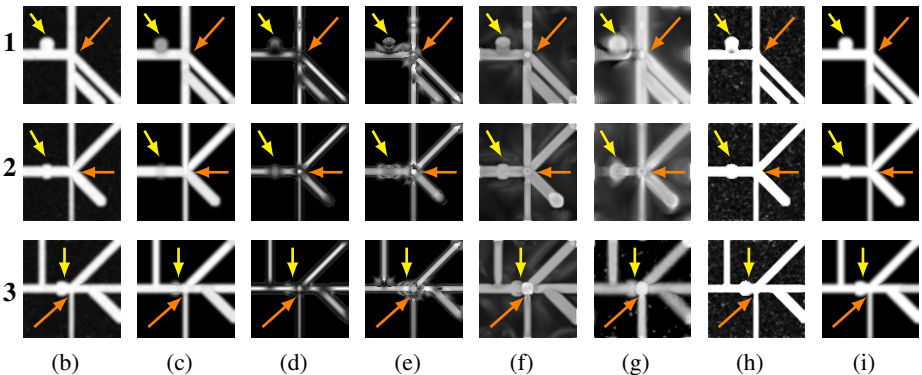


Figure 4: Comparison of methods' responses to vessels, intersections/junctions, and blobs. A 3D synthetic image (a) by 100x100x100 voxel is generated and three angle 2D max intensity projection is used (b); respectively 1st row is X, the 2nd row is Y and the 3rd row is Z direction. All vessels have nine pixel thickness and blob has a diameter of 21 pixel. (c) shows the bowler-hat and the state-of-the-art methods respectively, (d) vesselness, (e) neuriteness, (f) PCT vesselness, (g) PCT neuriteness, (h) volume ratio, and (i) RORPO. The arrows refer features of interest: blob-like structures (yellow arrows), junctions (orange arrows), noise (green arrows).

4.5 Response to Vessels, Intersections/Junctions, and Blobs

Figure 4 illustrates the comparison between the proposed method and state-of-the-art methods. It is obvious that most of the state-of-the-art methods fail at the junction like in Figure 4d and some of those create false vessels effects as in Figure 4g or add noise the enhance image Figure 4h. Compare to others, our proposed method is free from all of these effects and artefacts, but it is not good at suppressing the blob-like structures as like vesselness or neuriteness.

4.6 Response to Vascular Network Complexity

Nine volumetric images and their corresponding ground truth images of 3D synthetic vascular networks with an increasing complexity were generated using the VascuSynth Soft-

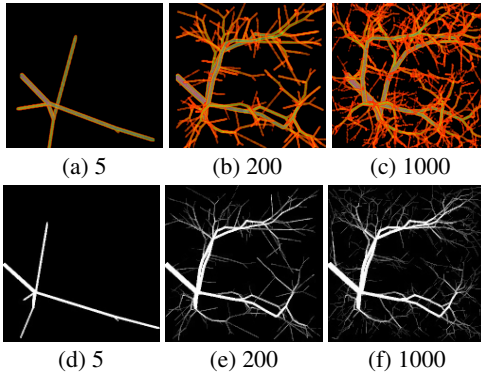


Figure 5: Visualisation of 3D synthetic vascular networks images generated with the VasuSynth Software [14]. The images (a-c) (167x167x167 voxels) are used to quantitatively validate the proposed method and the state-of-the-art methods and (d-f) are the result of the proposed method results. More detailed results are shown in Figure 6 and in Table 1.

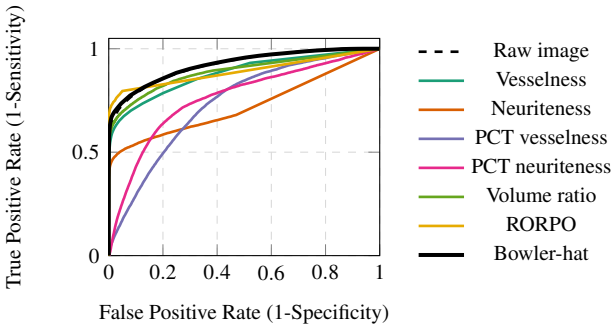


Figure 6: Mean ROC curve for all vascular networks images from Figure 5 calculated using the proposed and the state-of-the-art methods (see legend for colours). Individual AUC values can be found in Table 1.

ware [14], as shown in Figure 5. In addition, to make the image more realistic, we add a small amount of the Gaussian noise of level $\sigma_2 = 10$ and apply a Gaussian smoothing kernel with a standard deviation of 1. We tested the proposed methods as well as the aforementioned other approaches on these images. The results are presented in Table 1. Figure 6 also demonstrates the ROC curve all over the nine enhanced images. It appears that the proposed method clearly has the highest AUC value (0.965) compare to the state-of-the-art methods. Overall, the proposed method performance is better than the state-of-the-art methods.

4.7 Real Data

An Olfactory Projection Fibers image dataset from DIADEM Challenge [9] is used to demonstrate the robustness of proposed method against the noise. In two exemplary fibers images, a Gaussian noise was introduced at the noise levels ranging from $\sigma = 10$ to $\sigma = 60$, and salt and pepper noise at the different level of density $\rho = 10$ to $\rho = 60$ see Figure 7. Such images were then enhanced with the proposed method and the AUC values were calculated and presented in Figure 7. We also tested the performance of the proposed method on 3D real images. Here we adopt three representative types of real images, namely microcomputers network in plant cell, keratin network in skin cell, and neuronal network. Correspondingly we compare the output of the proposed method with five other approaches, and the results are shown in Figure 8. It is clearly suggested that our method has the best performance in preserving junctions.

Nodes	AUC						
	Vesselness	Neuritiness	PCT ves.	PCT veu.	Volume ratio	RORPO	Bowler-hat
5	0.999	0.923	0.840	0.897	0.999	0.999	0.999
10	0.996	0.883	0.820	0.873	0.998	0.997	0.999
50	0.976	0.830	0.794	0.851	0.981	0.965	0.994
100	0.951	0.778	0.778	0.827	0.957	0.930	0.982
200	0.930	0.755	0.770	0.799	0.936	0.900	0.966
400	0.910	0.746	0.749	0.788	0.917	0.879	0.950
600	0.902	0.743	0.742	0.777	0.909	0.869	0.941
800	0.885	0.719	0.724	0.756	0.893	0.855	0.926
1000	0.884	0.722	0.726	0.759	0.891	0.852	0.924
mean(std)	0.937(0.045)	0.788(0.073)	0.771(0.04)	0.814(0.05)	0.942(0.043)	0.916(0.058)	0.965(0.03)

Table 1: AUC values for nine 3D image of vascular networks with increasing network’s complexity (see Figure 5) enhanced with the proposed and the state-of-the-art methods. Best results for each vascular network are in bold. ROC curve of the all volumetric images can be seen in Table 6.

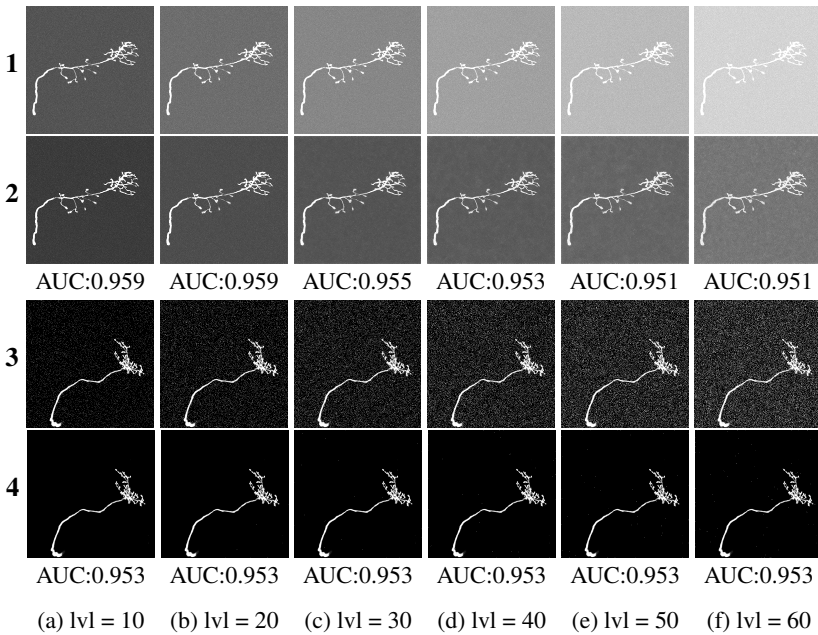


Figure 7: Application of the proposed method into the Olfactory Projection Neuron dataset from the DIADEM Challenge. All of the images are 2D maximum intensity projections. (1,3) Input images that have been contaminated by different levels (increasing left to right) and types of noise (1 - Gaussian additive noise; 3 - salt and pepper noise). (2,4) Enhancement results with the proposed method and corresponding AUC values.

5 Conclusion

Hessian- or Phase Congruency Tensor-based image enhancement methods had been commonly used to enhance vessel-like structures in 3D biomedical images using measurements like vesselness, neuritiness and volume ratio.

This paper proposes a novel mathematical morphology-based method for vessel-like structures enhancement in 3D biomedical images. The proposed method is shown to have benefits over existing methods, including no loss of signal and junctions and minimized artifacts at vessel ends. We show efficiency on both synthetic and real image datasets.

Future continuations of this work will introduce the implementation of the blob-enhancing variants of this concept.

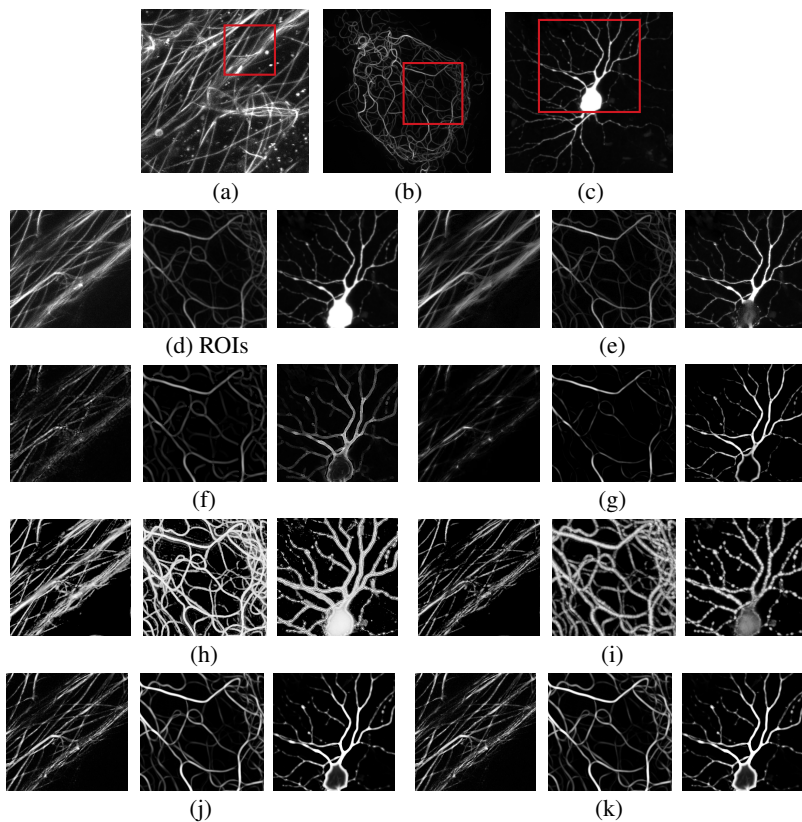


Figure 8: Comparison of the proposed and the state-of-the-art methods on a set of real biomedical images. 2D max projections of 3D images of microtubules network in plant cell (a), keratin network in skin cell (b) (provided by Dr Tim Hawkins, Durham University, UK), and neuronal network (c) (provided by Dr Chris Banna, UC Santa Barbara, USA). Regions of interest are highlighted in red and presented in (d). Results: bowler-hat (e), neuriteness (f), vesselness (g), PCT neuriteness (h), PCT vesselness (i), volume ratio (j), RORPO (k).

References

- [1] Yousef Al-Kofahi, Natalie Dowell-Mesfin, Christopher Pace, William Shain, James N Turner, and Badrinath Roysam. Improved detection of branching points in algorithms for automated neuron tracing from 3D confocal images. *Cytometry Part A*, 73(1):36–43, 2008.
- [2] Fethallah Benmansour and Laurent D. Cohen. Tubular structure segmentation based on minimal path method and anisotropic enhancement. *International Journal of Computer Vision*, 92(2):192–210, 2011.
- [3] PS Bijith and T Deepa. Image enhancement and 3-D reconstruction of coronary artery from multiple cardiac angiograms. *International Journal of Innovative Research in Science, Engineering and Technology*, 6(6), 2017.
- [4] Kerry M Brown, Germán Barrionuevo, Alison J Canty, Vincenzo De Paola, Judith A Hirsch, Gregory SXE Jefferis, Ju Lu, Marjolein Snippe, Izumi Sugihara, and Giorgio A Ascoli. The diadem data sets: representative light microscopy images of neuronal

- morphology to advance automation of digital reconstructions. *Neuroinformatics*, 9(2-3):143–157, 2011. 414
415
416
- [5] T. Chen, Q.H. Wu, R. Rahmani-Torkaman, and J. Hughes. A pseudo top-hat mathematical morphological approach to edge detection in dark regions. *Pattern Recognition*, 35(1):199–210, 2002. 417
418
419
- [6] Ricardo J Ferrari, Stéphane Allaire, Andrew Hope, John Kim, David Jaffray, and Vladimir Pekar. Detection of point landmarks in 3D medical images via phase congruency model. *Journal of the Brazilian Computer Society*, 17(2):117–132, 2011. 420
421
422
423
- [7] Alejandro F Frangi, Wiro J Niessen, Koen L Vincken, and Max A Viergever. Multiscale vessel enhancement filtering. In *International Conference on Medical Image Computing and Computer-Assisted Intervention*, volume 1496, pages 130–137, 1998. 424
425
426
427
- [8] Stathis Hadjidemetriou, Derek Toomre, and James S Duncan. Segmentation and 3d reconstruction of microtubules in total internal reflection fluorescence microscopy (tirmf). In *International Conference on Medical Image Computing and Computer-Assisted Intervention*, pages 761–769. Springer, 2005. 428
429
430
431
- [9] Karimollah Hajian-Tilaki. Receiver operating characteristic (ROC) curve analysis for medical diagnostic test evaluation. *Caspian Journal of Internal Medicine*, 4(2):627, 2013. 432
433
434
435
- [10] Ghassan Hamarneh and Preet Jassi. Vascusynth: Simulating vascular trees for generating volumetric image data with ground truth segmentation and tree analysis. *Computerized Medical Imaging and Graphics*, 34(8):605–616, 2010. 436
437
438
439
- [11] Andrei C. Jalba, Michael H.F. Wilkinson, and Jos B.T.M. Roerdink. Morphological hat-transform scale spaces and their use in pattern classification. *Pattern Recognition*, 37(5):901–915, 2004. 440
441
442
- [12] T. Jerman, F. Pernus, B. Likar, and Z. Spiclin. Enhancement of vascular structures in 3D and 2D angiographic images. *IEEE Transactions on Medical Imaging*, 35(9):2107–2118, 2016. 443
444
445
446
- [13] Asma Kerkeni, Asma Benabdallah, Antoine Manzanera, and Mohamed Hedi Bedoui. A coronary artery segmentation method based on multiscale analysis and region growing. *Computerized Medical Imaging and Graphics*, 48:49–61, 2016. 447
448
449
- [14] Cheng Guan Koay. Analytically exact spiral scheme for generating uniformly distributed points on the unit sphere. *Journal of Computational Science*, 2(1):88–91, 2011. 450
451
452
- [15] Peter Kovési. *Invariant measures of image features from phase information*. PhD thesis, University of Western Australia, 1996. 453
454
455
- [16] Peter Kovési. Image features from phase congruency. *Journal of Computer Vision Research*, 1(3):1–26, 1999. 456
457
- [17] Tony Lindeberg. *Scale-space theory in computer vision*, volume 256. Springer Science & Business Media, 2013. 458
459

- [18] E Meijering, M Jacob, J-CF Sarria, Pl Steiner, H Hirling, and M Unser. Design and validation of a tool for neurite tracing and analysis in fluorescence microscopy images. *Cytometry Part A*, 58(2):167–176, 2004.
- [19] Odysée Merveille, Hugues Talbot, Laurent Najman, and Nicolas Passat. Curvilinear structure analysis by ranking the orientation responses of path operators. *IEEE Transactions on Pattern Analysis and Machine Intelligence*, 40(2):304–317, 2018.
- [20] Sandra Morales, Valery Naranjo, Jesús Angulo, and Mariano Alcañiz. Automatic detection of optic disc based on pca and mathematical morphology. *IEEE Transactions on Medical Imaging*, 32(4):786–796, 2013.
- [21] M Concetta Morrone, John Ross, David C Burr, and Robyn Owens. Mach bands are phase dependent. *Nature*, 324(6094):250–253, 1986.
- [22] Boguslaw Obara, Mark Fricker, David Gavaghan, and Vicente Grau. Contrast-independent curvilinear structure detection in biomedical images. *IEEE Transactions on Image Processing*, 21(5):2572–2581, 2012.
- [23] Sonia H Contreras Ortiz, Tsuicheng Chiu, and Martin D Fox. Ultrasound image enhancement: A review. *Biomedical Signal Processing and Control*, 7(5):419–428, 2012.
- [24] Çiğdem Sazak and Boguslaw Obara. Contrast-independent curvilinear structure enhancement in 3D biomedical images. In *International Symposium on Biomedical Imaging*, pages 1165–1168, 2017.
- [25] Çiğdem Sazak, Carl J Nelson, and Boguslaw Obara. The multiscale bowler-hat transform for blood vessel enhancement in retinal images. *arXiv preprint arXiv:1709.05495*, 2017.
- [26] Jean Serra. Introduction to mathematical morphology. *Computer Vision, Graphics, and Image Processing*, 35(3):283–305, 1986.
- [27] Pierre Soille. *Morphological image analysis: principles and applications*. Springer Science & Business Media, 2013.
- [28] Ran Su, Changming Sun, Chao Zhang, and Tuan D. Pham. A new method for linear feature and junction enhancement in 2D images based on morphological operation, oriented anisotropic Gaussian function and Hessian information. *Pattern Recognition*, 47(10):3193–3208, 2014.
- [29] Wei Wang, Jianwei Li, Feifei Huang, and Hailiang Feng. Design and implementation of Log-Gabor filter in fingerprint image enhancement. *Pattern Recognition Letters*, 29(3):301–308, 2008.
- [30] F. Zana and J. C. Klein. Segmentation of vessel-like patterns using mathematical morphology and curvature evaluation. *IEEE Transactions on Image Processing*, 10(7):1010–1019, 2001.
- [31] Fan Zhang, Xinhong Zhang, Xianxing Liu, Kui Cao, Haishun Du, and Yanbin Cui. Blood vessel enhancement for dsa images based on adaptive multi-scale filtering. *Optik-International Journal for Light and Electron Optics*, 125(10):2383–2388, 2014.